

A new method for estimating the pattern speed of spiral structure in the Milky Way

T. C. Junqueira^{1*}, C. Chiappini¹, J. R. D. Lépine², I. Minchev¹, B. X. Santiago^{3,4}

¹Leibniz-Institut für Astrophysik Potsdam, An der Sternwarte 16, 14482 Potsdam, Germany

²Instituto de Astronomia, Geofísica e Ciências Atmosféricas, Universidade de São Paulo, Cidade Universitária, São Paulo 05508-090, SP, Brazil

³Instituto de Física, UFRGS, CP 15051, Porto Alegre, RS 91501970, Brazil

⁴Laboratório Interinstitucional de e-Astronomia-LIneA, Rua Gal. José Cristino 77, Rio de Janeiro, RJ 20921-400, Brazil

ABSTRACT

In the last few decades many efforts have been made to understand the effect of spiral arms on the gas and stellar dynamics in the Milky Way disc. One of the fundamental parameters of the spiral structure is its angular velocity, or pattern speed Ω_p , which determines the location of resonances in the disc and the spirals' radial extent. The most direct method for estimating the pattern speed relies on backward integration techniques, trying to locate the stellar birthplace of open clusters. Here we propose a new method based on the interaction between the spiral arms and the stars in the disc. Using a sample of around 500 open clusters from the *New Catalogue of Optically Visible Open Clusters and Candidates*, and a sample of 500 giant stars observed by APOGEE, we find $\Omega_p = 23.0 \pm 0.5 \text{ km s}^{-1} \text{ kpc}^{-1}$, for a local standard of rest rotation $V_0 = 220 \text{ km s}^{-1}$ and solar radius $R_0 = 8.0 \text{ kpc}$. Exploring a range in V_0 and R_0 within the acceptable values, 200-240 km s^{-1} and 7.5-8.5 kpc , respectively, results only in a small change in our estimate of Ω_p , that is within the error. Our result is in close agreement with a number of studies which suggest values in the range 20-25 $\text{km s}^{-1} \text{ kpc}^{-1}$. An advantage of our method is that we do not need knowledge of the stellar age, unlike in the case of the birthplace method, which allows us to use data from large Galactic surveys. The precision of our method will be improved once larger samples of disk stars with spectroscopic information will become available thanks to future surveys such as 4MOST.

Key words: stars: kinematics and dynamics – Galaxy: structure.

1 INTRODUCTION

The Milky Way (MW) has long been known to possess spiral structure, but its fundamental nature is still under debate today. In the classical spiral structure theory of Lin & Shu (1964), as well as other models which consider that the spiral arms are caused by the crowding of stellar orbits (e.g. Kalnajs 1973; Contopoulos & Grosbol 1986; Pichardo et al. 2003; Junqueira et al. 2013), the spiral arm pattern rotates like a rigid body with a well defined angular velocity Ω_p . In these models Ω_p is usually treated as a free parameter to be determined by observations. However, its value has a crucial importance on the understanding of Galactic dynamics and evolution, since it determines the place of resonances in the disc, for a given rotation curve. In addition to this challenge, there are also theories of spiral arms claiming that the pat-

tern speed and pitch angle are variable (Toomre 1981), that spirals are transient phenomena on a rotational time scale (e.g., Sellwood & Binney 2002), or that there exist at any time several spiral sets with distinct pattern speeds overlapping in radius e.g., Masset & Tagger 1997; Merrifield et al. 2006; Quillen et al. 2011; Minchev et al. 2012, or even that the spiral arms are stochastic phenomena e.g., Patsis 2006.

Looking at the existing theories, we can see that it is not clear whether the Ω_p can be described by a multiple, transient or a constant pattern speed. However, some authors have shown that the corotation radius is close to the solar orbit (Marochnik et al. 1972; Creze & Mennessier 1973; Mishurov & Zenina 1999; Dias & Lépine 2005). Amôres et al. (2009) associated a gap in the Galactic HI distribution close to the corotation radius, while Scarano & Lépine (2013) showed a break in the radial metallicity gradient close to the corotation radius for many external galaxies. This suggests that we have dominant spiral arms with a constant pattern

* E-mail: tjunqueira@aip.de

speed for, at least, a few billion years, which do not support models with transient spiral arms that survive for only a few galactic rotations at the solar radius. Thus, the approximation of a single and steady pattern speed is a useful first step to see whether this assumption is consistent with available data.

The most direct method to measure the pattern speed of the MW relies on the birthplaces of the observed open clusters. It is done by integrating backwards in time their orbits according to their known location, ages and circular velocity in the disk. Assuming that the open clusters are born in spiral arms, the distribution of birthplace for some age bins should be spiral-like (where we assume logarithmic spirals), and by comparing the spiral patterns obtained from different ages bins, the rotation rate of the spiral arms can be estimated. This is a valuable way to measure the pattern speed, but determining ages for a large open cluster sample is not an easy task and may introduce large errors.

In the present work, we introduce a new method to determine the angular velocity Ω_p based on the interaction between the stars and the spiral arms, that cause an exchanged of energy and angular momentum (we use energy and angular momentum per mass unit, but for simplicity we keep the terminology energy and angular momentum). The only assumption made in this method is that the initial energy is the energy of a circular orbit placed at the mean radius r_m . We do not give any information a priori about the spiral arms, which is already included in the velocities components of each object. Moreover, we do not need to know the ages or make any assumption about the spiral arms shape. In addition, the fact that we do not have to make use of ages allows us to use observational data that provide only positions and kinematics information, and hence can be a powerful method in the era of large spectroscopic surveys such APOGEE-2 (as part of SDSS-IV - [Sobeck et al. \(2014\)](#)), and future very-large ones as 4MOST¹ and WEAVE².

The organization of this paper is as follows: in Section 2 we present the new method for measuring the spiral pattern speed of the Galaxy. In this same Section we provide the rotation curve used to compute the Galactic potential and how the mean radius is calculated for each object, as well as some tests made to validate the method. In Section 3, we describe the data used to compute Ω_p . In Section 4, we compare our result with the ones found in the literature and discuss possible sources of errors. Concluding remarks can be found in Section 5.

2 METHOD

As a star travels around the Galactic center it interacts with the spiral arms, which results in exchange of angular momentum and energy. The rate at which this happens depends on the relative angular velocity $\Omega - \Omega_p$, where Ω is the observed stellar angular velocity. Thus, in an inertial frame of reference, the energy of a star varies due to perturbations caused by the presence of the spiral arms but, if there is only one pattern speed, we can find a Hamiltonian that is time independent. This Hamiltonian system lies on the frame of

reference of the spiral arms, which is a non-inertial frame of reference. This is known as the Jacobian of the system ([Binney & Tremaine 2008](#)), written as:

$$H = E - \Omega_p J, \quad (1)$$

where H is the energy in the non-inertial frame of reference, while E and J are the energy and the angular momentum in the inertial frame of reference, respectively. The energy of star E is given by:

$$E = \frac{1}{2} \left(U^2 + \frac{J^2}{r^2} \right) + \Phi_0(r) + \Phi_1(r, \theta), \quad (2)$$

and

$$J = r^2 \Omega, \quad (3)$$

U is the radial velocity toward the Galactic center, r is the star's distance from the Galactic center, $\Omega = V/r$ where V is the rotational velocity, $\Phi_0(r)$ is the axisymmetric potential and $\Phi_1(r, \theta)$ is the perturbative potential due to spiral arms. Once the total energy H is conserved ($\Delta H = 0$) we can derive, from Eq. 1, that the energy variation for each star is proportional to the angular momentum variation;

$$\Delta E = \Omega_p \Delta J. \quad (4)$$

Eq. 4 is not new and it was obtained also by [Lynden-Bell & Kalnajs \(1972\)](#) and [Sellwood & Binney \(2002\)](#). The process of steady angular momentum transfer between the spiral density and a star in resonant motion with the perturbation is understood in the following way: the loss (gain) of angular momentum ΔJ by a star at the inner Lindblad resonance is accompanied by the loss of energy $\Omega_p \Delta J$; at the same time, the change in orbital energy, relative to the circular motion, is $\Omega \Delta J$, which is less than $\Omega_p \Delta J$. The connection between the orbital energy E and angular momentum J is shown by Eq. 2, where for a pure circular motion it becomes $E_c = J^2/(2r^2) + \Phi_0(r)$, thus any variation in orbital energy leads to a variation in angular momentum at a rate proportional to the stellar angular velocity Ω . Thus the amount of energy in radial direction ΔE_r acquired by the star appears as non-circular motion:

$$\Delta E_r = (\Omega_p - \Omega) \Delta J, \quad (5)$$

We can merge Eqs. 4 and 5 into the following:

$$\Delta E_r + \Delta E + \Omega \Delta J = 2 \Delta J \Omega_p. \quad (6)$$

The challenge here is to find ΔE_r , ΔE , and ΔJ for a real set of stars in the Galaxy. The first consideration that we can make is that the axisymmetrical potential and the kinetic energy are larger than the perturbation, thus we might ignore the term $\Phi_1(r, \theta)$ from Eq. 2. This is justifiable because the residual velocities of the objects in comparison with the pure circular ones already carries information about the perturbing field, and another important reason is that we are not giving any prior information about the spiral

¹ 4-m multi-object spectrograph telescope - [de Jong et al. \(2012\)](#)

² <http://www.ing.iac.es/weave/index.html>

arms. Thus we can rewrite Eq. 2 ignoring the perturbative term;

$$E \simeq \frac{1}{2} \left(U^2 + \frac{J^2}{r^2} \right) + \Phi_0(r). \quad (7)$$

When we observe a star we just have access to its energy and angular momentum at one specific period, in other words, we cannot track a star for a few millions of years to see how it will change its energy and angular momentum over time. In an idealized case, where we know exactly the values of ΔE and ΔJ (e.g. in a simulation), we could use Eq. 4 to recover Ω_p . However, the problem of not knowing the exact values of ΔE and ΔJ introduces errors in this computation. This is why we make use of Eq. 6, which is the combination of Eqs. 4 and 5, forcing both equations to be satisfied giving us a better result. We also average the values of $y = \Delta E_r + \Delta E + \Omega \Delta J$ and $x = 2\Delta J$ for all stars inside a bin, which improves our results as explained below. It is important to emphasize that we bin the mean radius of the stars and not the actual radial position.

To solve the problem of the unknown ΔE and ΔJ , we assume that the initial energy E_0 and angular momentum J_0 of each star is the energy of a circular orbit at the mean radius r_m (Eq. 21 gives the definition of r_m):

$$E_0 = \frac{J_0(r_m)^2}{2r_m^2} + \Phi_0(r_m), \quad (8)$$

with

$$J_0 = r_m V_c(r_m), \quad (9)$$

where V_c is the rotation curve supplied by Eq. 18. Now we have all the necessary ingredients to compute the variation in energy and angular momentum:

$$\Delta E_i = E_i - E_{0i} = \frac{U_i^2}{2} + \frac{V_i^2 - V_c^2(r_{m_i})}{2} + \Delta\Phi_0(r_i - r_{m_i}), \quad (10)$$

$$\Delta J_i = J_i - J_{0i} = r_i V_i - r_{m_i} V_c(r_{m_i}), \quad (11)$$

and

$$\Delta E_{r_i} = \frac{U_i^2 - U_{max}^2}{2}. \quad (12)$$

The sub-index i refers to each star, V_i and U_i are respectively, the observed circular velocity and the radial velocity with respect to the center of the Galaxy, and U_{max} is the maximum radial velocity, that happens when the star crosses r_m . Both velocities V_i and U_i , are not directly observables, what we observe directly are the proper motion and the heliocentric velocity, to make this transformation we follow Johnson & Soderblom (1987). To correct the motion due to the local standard rest (LSR) we used the values from Schönrich et al. (2010); $u_0 = -11.1 \text{ km s}^{-1}$ and $v_0 = 12.24 \text{ km s}^{-1}$.

The next step is to bin the mean radius in intervals of $\Delta r = 0.2 \text{ kpc}$ from 5 up to 14 kpc. The reason for it is that stars with similar mean radius are expected to have almost the same energy H , which reflect the initial energy of

a circular orbit in which the star could have come from (see Section 2.1 for a better explanation). Therefore, inside each bin we have a number N of stars within $r < r_m < r + \Delta r$ and we average ΔE_i , ΔJ_i and ΔE_{r_i} for all the N stars within the bin. Thus Eq. 6 can be rewritten as:

$$\Delta \bar{E} = 2\Omega_p \Delta \bar{J}, \quad (13)$$

where $\Delta \bar{E}$ and $\Delta \bar{J}$ give us the energies and the angular momentum variation in each bin;

$$\Delta \bar{E} = \frac{1}{N} \sum_{i=1}^N (\Delta E_i + \Delta E_{r_i} + \Omega_i \Delta J_i), \quad (14)$$

and

$$\Delta \bar{J} = \frac{1}{N} \sum_{i=1}^N \Delta J_i. \quad (15)$$

Thereby, using Eq. 13, we can recover the value of Ω_p without giving any previous input about the perturbation by fitting a first degree equation $y = ax + b$. Where, $y = \Delta \bar{E}$ and $x = 2\Delta \bar{J}$, with a and b as free parameters. The slope of this fit give us the value of Ω_p .

In Section 2.1 we show how we compute the mean radius and the rotation curve. In Section 2.2 we carry out tests based on simulated particles in order to show our method works, and to estimate the expected uncertainty on the retrieved Ω_p parameter.

2.1 Assumptions of the method and uncertainties

We critically discuss the main assumptions of our method and their impact on the recovered Ω_p value. The main assumption of our method is that there is a dominant pattern speed that lasts, at least, for a few billion years. Notice that all existing methods are based on this premise.

As stated before, in a real sample we don't have access to the true variation in energy and angular momentum of each star. To overcome this problem another main assumption made here is that the initial energy E_0 and the initial angular momentum J_0 , come from a circular orbit placed at the mean radius (see Fig. 1). In a pure circular orbit all the stars at the same radius have the same energy and angular momentum as those quantities depend only on the stellar position (see Eqs. 8 and 9). We then split our sample in bins of mean radius (as stars with similar mean radius will have, according to our assumption, similar initial energy E_0 and angular momentum J_0). The bin width we chose was 0.2 kpc, to assure that the Eqs. 8 and 9 do not vary too much and at the same time we could have enough stars (at least more than 5) in each bin. We next discuss the impact radial migration would have on this important assumption of our method.

Minchev et al. (2013) showed that in a simulated disk similar to the Milky Way migration is a global process, significantly affecting the entire disk. How would this affect our results, in particular the relation $\Omega_p = \Delta E / \Delta J$? We expect that the impact of migration on our method will be small for the following reasons. Minchev et al. (2012) showed that, due to conservation of vertical and radial actions, migrators

Table 1. Parameters of the rotation curve (Eqs. 18 and 19).

α	β	γ	δ	ϵ	η	A_{mrc}	R_{mrc}	σ_{mrc}
[km s ⁻¹]	[kpc]	[kpc]	[km s ⁻¹]	[kpc]	[kpc]	[km s ⁻¹]	[kpc]	[kpc]
250	120	3.4	360	3.1	0.09	20	8.8	0.8

arrive at a new radial location with orbital properties very similar to the stars which did not migrate. Therefore, the ΔE and ΔJ values at the final migration time are expected to be very similar to those of the local non-migrators. An exception to this rule would come from stars currently in the process of migration. While those could be a large number at high redshift due to the strong effect of external perturbers (e.g., large infalling satellites), it should be expected that at present these "migrators in action" do not constitute a significant fraction of the stars found in a given radial bin.

Another possible source of error can result from kinematically hot stars, i.e., stars with high eccentricity, for which our main assumption that the initial energy E_0 and the initial angular momentum J_0 , come from a circular orbit at the mean radius r_m , starts being imprecise. This is the main reason for using averaged ΔE and ΔJ values for stars sharing the same bin in mean radius. Because the stars with hot kinematics are mostly old, we adopt a) a sample of open clusters for which only 8% have ages above 1 Gyr (see Fig. 3), b) a stellar sample confined to the Galactic plane, mostly dominated by thin disk stars and c) spiral arms have the strongest dynamical effect in the disk midplane and thus stars with low vertical oscillations are the best tracers for the arms. As we discuss in the Results Section, the fact that we obtain very similar results from both samples, show the impact of the above mentioned shortcomings (radial migration and stars on eccentric orbits) in our method to be minor.

Finally, the main source of error in our method comes from the computation of ΔE and ΔJ . To illustrate how the errors from ΔE and ΔJ affect the measurement of Ω_p , we propagate the errors using the Eq. 4 and we derived the equation below:

$$\sigma_{\Omega_p} = \frac{1}{\Delta J} \sqrt{\sigma_{\Delta E}^2 + \frac{\Delta E^2}{\Delta J^2} \sigma_{\Delta J}^2}. \quad (16)$$

It simplify the analysis once we assume that the major errors come only from ΔE and ΔJ . Here $\sigma_{\Delta J}$ and $\sigma_{\Delta E}$ are the errors from these two variables. Now let's assume that the errors follow the relation; $\sigma_{\Delta E} = \alpha \Delta E$ and $\sigma_{\Delta J} = \beta \Delta J$. This tell us that the errors are proportional to the own variation of energy and angular momentum, respectively. This makes sense because E_0 and J_0 become less precise when the variation of ΔE and ΔJ are larger. Thus, for the errors following the given definition we can rewrite the equation above as:

$$\sigma_{\Omega_p} = \frac{\Delta E}{\Delta J} \sqrt{\alpha^2 + \beta^2} = \Omega_p \sqrt{\alpha^2 + \beta^2}. \quad (17)$$

For a single star the parameters, α and β , can be larger than one, which leads to an error greater than 100% in Ω_p . However, the errors in α and β are much smaller once we use a large number of stars averaged on a particular mean radius bin. Indeed, for the test sample α and β are ≈ 0.1 ,

which can be seeing in the errors bar for ΔE in Fig. 2, for ΔJ the magnitude of the errors bar are the same. Thus, from Eq. 17 with $\alpha = \beta = 0.1$ and $\Omega_p = 23 \text{ km s}^{-1} \text{ kpc}^{-1}$ we have an error of $\sigma_{\Omega_p} = 3 \text{ km s}^{-1} \text{ kpc}^{-1}$. In a more general way $\sigma_{\Omega_p} = 0.14 \Omega_p \text{ km s}^{-1} \text{ kpc}^{-1}$

In summary, the oldest the population, the less precise is our method. On the other hand, a very young population (<10 Myrs), which most probably would not have had enough time to interact with the spiral arms, because of the transformation of dissipational to collisionless dynamics, can also lead to uncertain results. An optimal sample would be composed of stars with ages between 50 Myrs and a few Gyrs. Finally, as discussed before we expect larger errors for larger values of ΔE and ΔJ . Hence, larger uncertainties should be expected for stars migrating from the resonances (i.e. inner or outer Lindblad resonance, ILR or OLR), as these stars might have increased significantly their energy and angular momentum. The two samples adopted here were chosen with the aim to minimize these effects (see Section 3). Finally, we notice that a large number of stars per mean radius bin improves our determination of Ω_p .

2.2 Mean radius and the rotation curve

In order to find the mean radius we adopt a model for the axisymmetric galactic potential that reproduces the general behavior of the rotation curve of the Galaxy. We use an analytical expression to represent the circular velocity as a function of Galactic radius, conveniently fitted by exponential in the form (units are km s⁻¹ and kpc):

$$V_c(r) = \alpha \exp \left[-\frac{r}{\beta} - \left(\frac{\gamma}{r} \right)^2 \right] + \delta \exp \left[-\frac{r}{\epsilon} - \frac{\eta}{r} \right] + f_{\text{mrc}}(r), \quad (18)$$

with

$$f_{\text{mrc}}(r) = -A_{\text{mrc}} \exp \left[-\frac{1}{2} \left(\frac{r - R_{\text{mrc}}}{\sigma_{\text{mrc}}} \right)^2 \right], \quad (19)$$

where A_{mrc} is the amplitude and σ_{mrc} is the half-width of the minimum centered at the radius R_{mrc} . We verified that the adopted depth of the minimum in Eq. 19 does not have any measurable effect on the value of Ω_p obtained in this work. The rotation curve given by the expressions in Eqs. 18 and 19 is close to that derived by Fich et al. (1989) and is also similar to the ones previously used by, e.g., Lépine et al. 2008; ALM; Lépine et al. 2011a. The interpretation of a similar curve in terms of components of the Galaxy is given by Lépine & Leroy (2000). Table 1 gives the values of the parameters chosen to reproduce the rotation curve of the Milky Way. For the Galactocentric distance of the Sun, we adopt $R_0 = 8.0 \text{ kpc}$. The circular velocity at R_0 resultant

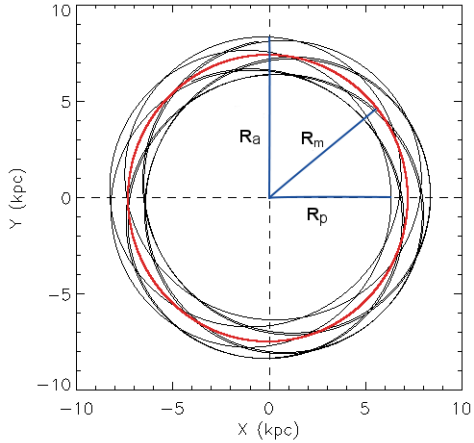


Figure 1. This figure illustrates a typical orbit, in an inertial frame of reference, where the star follows elliptical orbits which are confined in a circular region limited by the pericenter (r_p) and the apocenter (r_a). The black lines show the stellar orbit, the red line is the position of the mean radius r_m .

from Eq. 18 is $V_0 = 210 \text{ km s}^{-1}$, for a peculiar velocity of the Sun in the direction of Galactic rotation $v_0 = 12.24 \text{ km s}^{-1}$ the velocity with respect to the local standard rest is $V_{LSR} \simeq 220 \text{ km s}^{-1}$. For more details and also a theoretical description about the minimum close to the solar position see Barros et al. (2013).

As we restrict our study to orbits in the galactic plane, the axisymmetric potential can be derived directly from the rotation curve:

$$\Phi_0(r) = \int \frac{V_c^2}{r} dr. \quad (20)$$

We integrated the stellar orbits for 2 Gyr under the influence of the potential $\Phi_0(r)$, excluding any perturbations. This allowed us to find the apocenter (r_a) and pericenter (r_p) radius. The mean radius is then given by;

$$r_m = \frac{r_a + r_p}{2}. \quad (21)$$

Fig. 1 shows an example of an orbit with the apocenter, pericenter and mean radius of a star in the Galactic potential.

2.3 Application of the method to modeled data

In order to test our method we integrate the orbits of 500 test-particles for 2 Gyr under the influence of a perturbing potential with a given value of Ω_p . We chose 500 particles to match with the number of stars we have available in each sample, approximately. With future data, the increase of these number and a better distributed in the Galactic plane, could improve the results, as we will discuss later in the Sec. 3. The potential and parameters that we used for the spiral arms are described in Junqueira et al. (2013) (their Eq. 6 with the parameter values given on their Tab. 1). The axisymmetric potential Φ_0 comes from Eq. 20, with the rotation curve V_c given by Eq. 18, where we set $\Phi_0(100)$

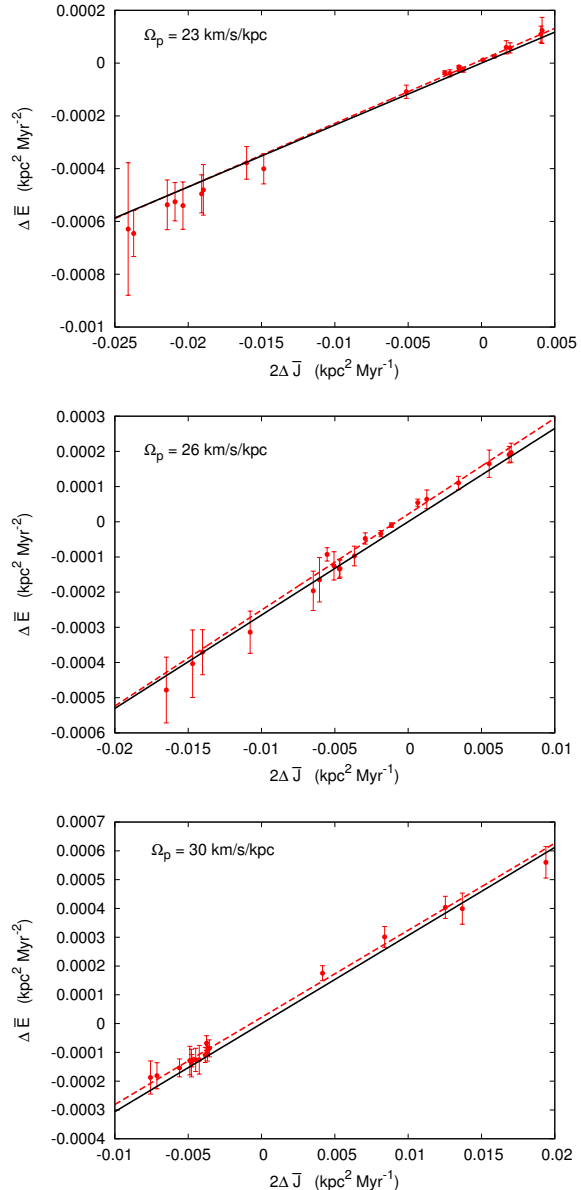


Figure 2. This figure shows the linear correlation between $2\Delta\bar{J}$ and ΔE for three different values of Ω_p . The red dots are the values computed from Eqs. 14 and 15, as explained in Sec. 2, the dashed red lines are the least-squares fit on these points, where the slope give us the value of Ω_p (shown on Tab. 2), and the black lines are the linear relation for the original value of Ω_p .

$= 0$ at $r = 100 \text{ kpc}$ to find the constant of integration. Initially, the test-particles were distributed between 6 and 12 kpc with random azimuthal positions, and initial circular velocities corresponding to the rotation curve V_c . The test-particles have initial radial velocities U , given by a Gaussian shape in each bin of radius and the half-width is the velocity dispersion σ_r that follows a radial profile given by Eq. 22.

$$\sigma_r = \sigma_{r_0} \exp\left(\frac{r_0 - r}{5}\right), \quad (22)$$

with $r_0 = 8 \text{ kpc}$ at the solar radius and a velocity dispersion $\sigma_{r_0} = 6.5 \text{ km/s}$. These values are compatible with the

Table 2. The first column shows the input value for Ω_p and the second column shows the value of Ω_p recovered by our method. All values in this table have units of $\text{km s}^{-1} \text{kpc}^{-1}$.

Input Ω_p	Recovered Ω_p
23	23.5 ± 0.9
26	26.7 ± 1.0
30	29.7 ± 0.7

amplitudes of the perturbation velocities due to the spiral waves found in the literature (e.g. [Burton 1971](#), [Mishurov et al. 1997](#), [Bobylev & Bajkova 2010](#)). They are also similar to the velocity dispersion of the youngest Hipparcos stars ([Aumer & Binney 2009](#)).

The second step is to recover the value of Ω_p from this synthetic sample that we generated. To do that we selected the particles from different snapshots in order to simulate different ages, as we have in a real sample. After that, we re-integrate the orbits using only the axisymmetric potential to find the mean radius of each particle. Then we use the method explained before to compute the Eqs. 14 and 15. In Fig. 2 we show the results obtained for different values of Ω_p , where the error bars are the RMS (root mean square) of each bin. Table 2 summarizes the results; the first column is the input values of Ω_p , the second column shows the recovered values, that are given by the slope of a least-squares fit shown in Fig. 2, with the respective asymptotic standard errors. We can see that our method is able to recover the value of Ω_p down to around 4% precision.

In Sec. 4 we will apply this method to a sample of open clusters and stars from Apogee catalog to compute the Ω_p of the MW spiral arms.

3 THE DATA

In this Section we describe the two data sets we adopt to illustrate our new proposed method for deriving the pattern speed of the spiral structure of the Milky Way. As discussed in Section 2.3 we are interested in a sample of stars and/or clusters dominated by young-intermediate age objects, mostly close to the Galactic plane and for which we have good distances, radial velocities and proper motion information. Here we adopt two samples, which have complementary advantages and disadvantages. In this way we are able to illustrate the robustness of our method. Indeed, as we will see in the Results section, the two samples lead to essentially the same results, despite their different azimuthal and age coverage. We now describe each of the samples.

3.1 Open Clusters

Open clusters play an important role on the study of Galactic dynamics, because they are mostly concentrated in the disc plane. Thus, we can use them to find evidences about the kinematic and evolution of the MW’s disc.

The open clusters that we used to measure the pattern speed of the spiral arms belong to the “New Catalog of Optically Visible Open Clusters and Candidates”, published

by [Dias et al. \(2002\)](#)(DAML02)³, version 3.3. This catalog is an update from the previous ones by, [Lynga & Palous \(1987\)](#) and [Mermilliod et al. \(1995\)](#), and contains 2140 objects with measured parameters such as distance (for 74.5% of the sample), age (74.5%), proper motion (54.7%) and radial velocity (24.2%). In this work we used 513 open clusters from this catalog, which have distance, proper motion and radial velocity available simultaneously. Fig. 3 shows the age distribution of our OC sample. It can be seen that most of the objects are confined in the 10-1000 Myr age range which is an ideal age range for applying our method (see discussion in Section 2.3). Finally, the mean radius distribution of our OC sample is shown in Fig. 4 (solid black line). The OC sample is concentrated in the 7-10 kpc mean radius range where the percentage of young stars coming from the resonance regions is expected to be small (see [Minchev et al. 2013, 2014](#)). For the OCs, [Paunzen & Netopil \(2006\)](#) show a limit of 20% in the errors for distances, which are similar to APOGEE HQ sample, and the errors in proper motion for 90% of our OCs sample are less than 1 mas/yr. The uncertainties in radial velocities are less than 5%.

3.2 APOGEE

The Apache Point Observatory Galactic Evolution Experiment (APOGEE; [Allende Prieto et al. 2008](#); [Majewski & The SDSS-III/APOGEE Collaboration 2014](#)), is one of the four Sloan Digital Sky Surveys III (SDSSIII; [Eisenstein et al. 2011](#)). Recently, [Anders et al. \(2014\)](#) have defined a subsample of the first year of APOGEE data (as part of data release 10, DR10; [Ahn et al. 2014](#)). The selection criteria for what the latter authors named their APOGEE High Quality Giant Sample are summarized in Table 1 of [Anders et al. \(2014\)](#).

Starting from a similar sample, we have selected stars that stay on the galactic plane (i.e. with their maximum vertical orbital amplitude, z_{max} , below 0.2 kpc. Moreover, we required a combined proper-motion error below 4 mas/yr ($\delta_{\mu_{RA}} < 4 \text{ mas/yr}$ and $\delta_{\mu_{DEC}} < 4 \text{ mas/yr}$, mean proper motion error in right ascension and declination, respectively). The final sample resulted in 559 stars from DR10 which is a subsample from what [Anders et al. \(2014\)](#) named their gold sample. The distances were computed using the distance code of Santiago (priv. communication - see also [Santiago et al. 2015](#)). The mean uncertainties of distances and proper motions for the APOGEE DR10 sample are shown by [Anders et al. \(2014\)](#), where their gold sample have a threshold in uncertainties of 20% in distances and 4 mas/yr in proper motion. Also for the APOGEE sample, the uncertainties in radial velocities are less than 5%. Their mean radius distribution are shown in Fig. 4 (dashed red histogram), and turned out to be similar to that of our sample of OCs. The main difference is that the APOGEE giants span, most probably a larger age range. Indeed, we expect stars with mean radius in the 7-10 kpc range to be predominantly of ages between 1 and 6 Gyrs (see [Minchev et al. 2014](#)). For consistency, for the final sample of APOGEE stars we recompute the mean radius r_m using the rotation curve given by Eq. 18

³ <http://www.astro.iag.usp.br/ocdb/>

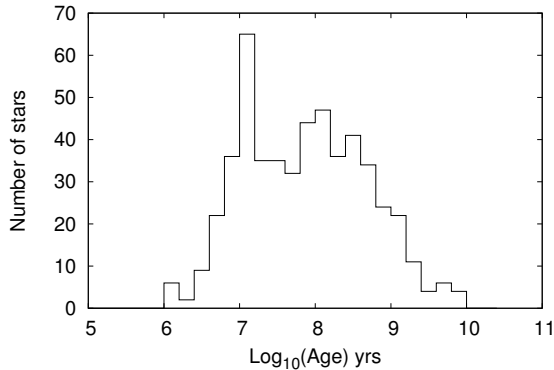


Figure 3. Logarithmic distribution of the ages for the OC's sample.

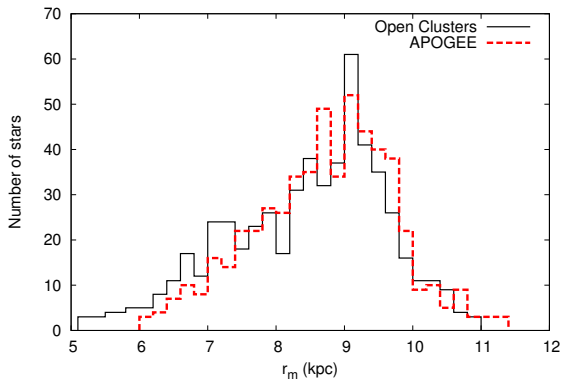


Figure 4. This figure shows the mean radius distribution of the OC sample (solid black curve) and red giant branch stars from APOGEE (dashed red curve). Both samples have similar distribution, as well as almost the same number of objects per bin.

instead of the one from [Anders et al. \(2014\)](#). However, in both calculations the mean radii are very similar.

Finally, in [Fig. 5](#) we show the spatial distribution of both samples on the X-Y Galactic plane. The first thing that can be noticed is that the OCs are more homogeneously distributed in the azimuthal direction than the APOGEE sample adopted here. The second difference is that we have more OCs in the inner part of the disk, while the APOGEE sample is more concentrated in the outer parts. This will certainly be improved once APOGEE-2 data will be available. As we will see in the next Section, despite these main differences, the pattern speed computed with both samples turned out to be very similar.

4 RESULTS AND DISCUSSION

In [Sec. 2](#) we described and tested a new method, without invoking any prior information about the spiral arms, which proved to be useful to constrain the value of the pattern speed within an error of $\sim 1 \text{ km s}^{-1} \text{ kpc}^{-1}$. Here we show the results that we obtain by applying our new method to a sample of disk stars and open clusters, described in [Sec. 3](#).

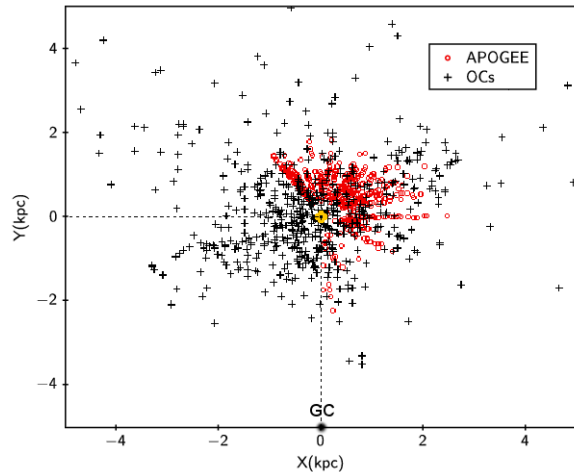


Figure 5. This figure shows the distribution in the X-Y galactic plane, with the Sun (yellow dot) locate in (0,0), for our adopted OC sample (black crosses) and red giant branch stars from APOGEE (red open circles). The Galactic center (GC) is pointed toward negative values in the Y-direction indicated by a black dot. We can see that the OC sample has a more wide azimuthal distribution than the giant branch stars from APOGEE (see text for more details).

4.1 The value of Ω_p and the corotation radius

Our main results are summarized in [Fig. 6](#), where we plot $2\Delta\bar{J}$ versus $\Delta\bar{E}$. The slope of the observed linear correlation gives the value of Ω_p (shown in [Tab. 4](#)), as described by [Eq. 13](#). The upper, middle and bottom panels show the results we obtain using the OC, red giants and the combination of the two, respectively. The color gradient indicates the center of the bin in radius in which each point. The value that we find by combining the two samples is $\Omega_p = 23.0 \pm 0.5 \text{ km s}^{-1} \text{ kpc}^{-1}$. For $\Omega_p = 23 \text{ km s}^{-1} \text{ kpc}^{-1}$ the corotation radius in our model is situated at $r_{cr} = (1.09 \pm 0.04)R_0$ which is in agreement with results found by [Dias & Lépine \(2005\)](#) with $r_{cr} = (1.06 \pm 0.08)R_0$. The fact that the Galaxy presents a well defined corotation radius supports the idea of a dominant pattern speed, at least, for an old stellar population (see further discussion in [Section 4.3](#)). It's interesting to notice that the values obtained for Ω_p from the fit, in [Fig. 2](#) or [Fig. 6](#), have unit of Myrs^{-1} . However the usual unit given for the pattern speed is in $\text{km s}^{-1} \text{ kpc}^{-1}$, thus to transform from (Myrs^{-1}) to ($\text{km s}^{-1} \text{ kpc}^{-1}$) we must divide by a factor of 0.00102.

We should keep in mind that our quoted uncertainties take into account only the fitting procedure. Systematic and intrinsic errors (e.g. assumptions made on the method and variation of the rotation curve because of uncertainties on the solar parameters R_0 and V_0) were not taken into account. However, we can estimate that by varying the values of R_0 and V_0 between $7 - 8.5 \text{ kpc}$ and $199 - 245 \text{ km s}^{-1}$ respectively. These variations would propagate into a $\sim 2 \text{ km s}^{-1} \text{ kpc}^{-1}$ change on the final value of Ω_p . [Piffl et al. \(2014\)](#) recently found $V_0 = 240 \text{ km s}^{-1}$ for $R_0 = 8.3 \text{ kpc}$, which is compatible with our adopted values and hence will change our estimate of Ω_p within the intrinsic errors. In [Sec. 2.1](#)

Table 3. Compilation of some estimations of Ω_p found in the literature.

Ω_p (km s ⁻¹ kpc ⁻¹)	Method*	Objects	Reference
19.1±3.6	1	Cepheids	Mishurov et al. (1979)
30±0.7	1	O and B-type stars and Cepheid	Fernández et al. (2001)
20±2	2	Open clusters	Amaral & Lépine (1997)
24±1	2	Open clusters	Dias & Lépine (2005)
20.3±0.5	2	Sample of runaways and early-type stars (from <i>Hipparcos</i>)	Silva & Napiwotzki (2013)
21.2±1.1	2	Only early-type stars	Silva & Napiwotzki (2013)
18.1±0.8	3	<i>Hipparcos</i> subsample	Quillen & Minchev (2005)
18.6±0.3	4	RAVE survey	Siebert et al. (2012)

*method 1 = kinematic model, method 2 = Birthplace technique, method 3 = Orbital analysis of moving group in the (u-v) plane,

*method 4 = Spiral perturbation to reproduce the gradient in the mean galactocentric radial velocity.

we discussed more about the intrinsic uncertainties of our method.

As we can see in the last panel in Fig. 6 the combination of both data, APOGEE + OCs, has a better distribution in $2\Delta\bar{J}$, this is due to a better spatial distribution when we combine the data. It happens because the stars have different values of radial velocities (and they do not belong to a group in a U-V velocity diagram) given us a better average of the angular momentum variation in an annular region of the disk. Thus, we expected that with the new coming data, from APOGEE-2 (now starting with SDSSIV), our results will improve, since it will increase the number of stars and in a way that the distribution in azimuth will become more homogenous. Another thing we can notice in this figure is that the points with higher $|2\Delta\bar{J}|$ and $|\Delta\bar{E}|$ come from mean radius around 6 or 12 kpc, that are very close to the IRL and OLR resonances and as we discussed before this regions warm up the disk.

4.2 Comparison with previous reported results in the literature

One of the most important parameters in studying the spiral structure is its pattern speed Ω_p . Although the fundamental nature of the spiral arms is not fully understood it plays an important role in galactic dynamics (e.g. Antoja et al. 2009; Lépine et al. 2011b; Quillen et al. 2011; Minchev et al. 2012; Sellwood 2014) and its pattern speed is a fundamental parameter that drives all the resonances in the disc. Table 3 summarizes the several previous attempts made in the literature to estimate the value of Ω_p . Gerhard (2011) made a review from the values found for the pattern speeds in the Milky Way and he end up with a range between $\Omega_p \sim 17-30$ km s⁻¹ kpc⁻¹.

As it is clearly seen from Table 3 and 4, our results are in agreement with studies that suggest a pattern speed between 20-25 km s⁻¹ kpc⁻¹. However, Quillen & Minchev (2005) and Siebert et al. (2012) found values bellow 20 km s⁻¹ kpc⁻¹, which are not in agreement with our results even with error bars around ~ 3 km s⁻¹ kpc⁻¹. In the literature we see that higher values for Ω_p are preferred by open cluster birthplaces while hydrodynamical simulations and phase space substructures favor slower pattern speeds. Thus, since Quillen & Minchev (2005) and Siebert et al. (2012) analysis are based on moving groups and the velocity gradient both close to the solar neighborhood, which are substructures

Table 4. This table contains our results for the pattern speed Ω_p obtained from two different samples and the combination of all them.

Ω_p (km s ⁻¹ kpc ⁻¹)	Sample
24.0±1.0	Open clusters
23.3±0.6	Apogee
23.0±0.5	Apogee + Open clusters

tures and can be associated only with one spiral structure (as e.g., Perseus arm or even a local spur arm), it could explain why they found lower values for Ω_p . The discrepancies of values found in the literature are discussed in Sec. 4.3, as a possible contamination by multiple spiral patterns, which are difficult to be taken into account and can lead to a systematic errors that explain the wide range of values found for Ω_p , depending on the tracers and the methods that were used to estimate it.

The value that we found for the dominant MW spiral pattern speed is also in agreement with the values found in many external galaxies. For example, Scarano & Lépine (2013) found Ω_p to have a distribution concentrated around 24 km s⁻¹ kpc⁻¹. However, the fundamental nature of the pattern speed is still not clear, which requires more theoretical work to be fully understood.

4.3 Possible contamination by multiple spiral patterns

Vallée (2014) uses many tracers to probe the spiral structure of our Galaxy and concludes that it has a four-armed spiral pattern. However, only two of these may be present in the density distribution of old stars (see, e.g. Drimmel 2000; Martos et al. 2004). Multiple spiral patterns could possibly be a source of errors when we try to determine only one pattern speed. Naoz & Shaviv (2007) measured the pattern speed for: Sagittarius-Carina and they found a superposition of two pattern speeds with $\Omega_p = 16.5 \pm 2.0$ km s⁻¹ kpc⁻¹ and $\Omega_p = 29.8 \pm 2.0$ km s⁻¹ kpc⁻¹, Perseus arm $\Omega_p = 20.0 \pm 2.0$ km s⁻¹ kpc⁻¹ and Orion $\Omega_p = 28.9 \pm 2.0$ km s⁻¹ kpc⁻¹. Some models also support multiple pattern speeds in order to explain radial migration in discs of galaxies (Minchev & Quillen 2006; Minchev et al. 2012; Grand et al. 2014). However others studies suggest that the MW has a corotation radius well established, situated close to

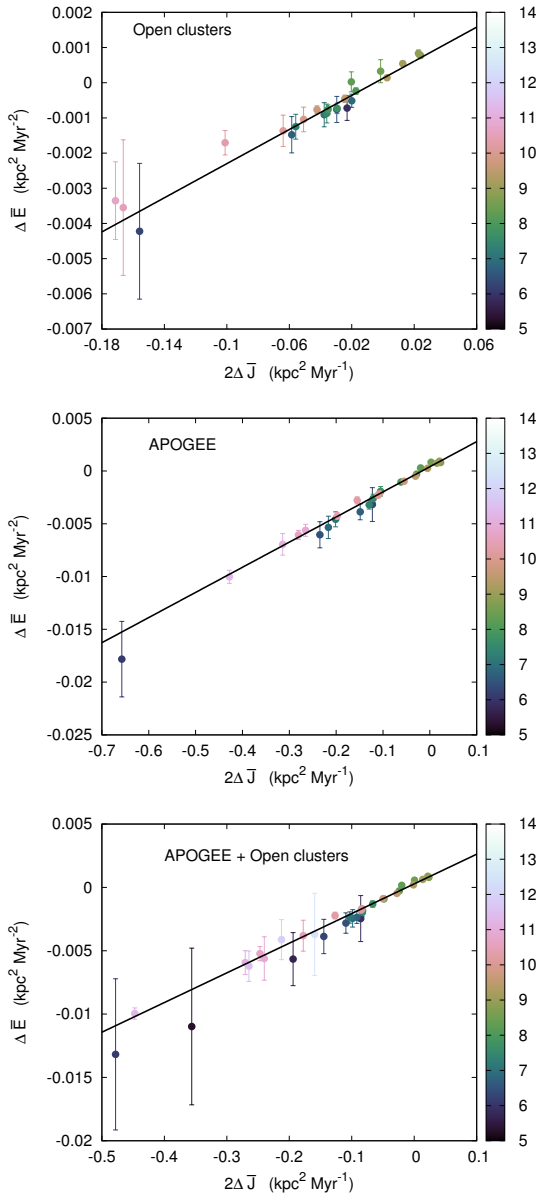


Figure 6. This figure shows the linear correlation between $2\Delta\bar{J}$ and $\Delta\bar{E}$ for a real sample. The dots are the values computed from Eqs. 14 and 15, as explained in Sec. 2, and the color code represent the bin radius in which each dot was computed. The black lines are the least-squares fit on these points, where the slope gives us the value of Ω_p . The upper panel shows the result for the OC sample; the middle shows the results for the APOGEE sample and the last one is the combination of both, APOGEE + OCs samples. The values of Ω_p found for each sample are shown on Tab. 4.

the solar radius (Marochnik et al. 1972; Creze & Mennessier 1973; Mishurov & Zenina 1999; Dias & Lépine 2005; Amôres et al. 2009, among others). It would be possible only if we have a dominant pattern speed rotating rigidly, nevertheless this do not exclude small structures to exist, that may rotate with different angular velocities. For $\Omega_p = 23 \text{ km s}^{-1} \text{ kpc}^{-1}$ the corotation radius in our model is situated at $r_{cr} = (1.09 \pm 0.04)R_0$ which is in agreement with results found by Dias & Lépine (2005) with $r_{cr} = (1.06 \pm 0.08)R_0$.

The fact that the Galaxy presents a well defined corotation radius supports the idea of a dominant pattern speed, at least, for an old stellar population. Therefore, one way to avoid a possible contamination by different pattern speeds is to split the sample into old and young stars.

In the future we will apply our method to a N-body simulation sample with multiple pattern speeds to check if we are able to distinguish multiple arms and/or analyze the influence of small arms on the dominant ones.

5 CONCLUSIONS

In this work, we proposed a new method to derive the spiral pattern speed of the MW based on the interaction between the spiral arms and the stellar objects. In this method we do not need any prior information about the spiral arms, as for example its shape and location. In addition, we do not need to be concerned with the stellar ages, which allows the use of data from large Galactic surveys.

The assumption we make in our method is that the initial energy and angular momentum of the objects can be approximated as the circular orbit at the mean radius. This approach introduces a natural error on the order of $1\sim 2 \text{ km s}^{-1} \text{ kpc}^{-1}$ which is equivalent, or even smaller, than the available methods to constrain the value of Ω_p .

Using a sample of open clusters and red giant stars from the APOGEE DR10 (Ahn et al. 2014) we have found $\Omega_p = 23.0 \pm 0.5 \text{ km s}^{-1} \text{ kpc}^{-1}$, which is compatible with other values in literature and placed the corotation radius at $r_{cr} = 8.74 \text{ kpc}$ for a solar position $R_0 = 8 \text{ kpc}$. We have to stress again that the given error for Ω_p here is just due to the RMS from the fitting procedure. A more realistic error estimate which also takes into account the errors intrinsic to our method should be around $2 \text{ km s}^{-1} \text{ kpc}^{-1}$ (intrinsic method error + RMS). Systematic errors and errors due to other sources of perturbation (as discussed in Sec. 4.3) are even more difficult to estimate, and could most probably explain the range of values for Ω_p , between $17 - 30 \text{ km s}^{-1} \text{ kpc}^{-1}$, found in the literature. Further studies, using N-body simulations data, are needed to check the effective influence of multiple spiral arms on the determination of Ω_p , assuming a constant pattern speed.

The new method for estimating the spiral pattern speed presented here can be tested with the large amounts of currently available data of ever increasing quality from large Galactic surveys, such as RAVE (Steinmetz et al. 2006), SEGUE (Yanny et al. 2009), APOGEE (Allende Prieto et al. 2008; Majewski & The SDSS-III/APOGEE Collaboration 2014), GES (Gilmore et al. 2012), and in the near future - Gaia (de Bruijne 2012), 4MOST (de Jong et al. 2012) and WEAVE (Dalton et al. 2012).

ACKNOWLEDGMENTS

I would like to tanks Douglas A. Barros for the comments and helpful discussions to improve this paper. TCJ is supported by DAAD-CNPq-Brazil through a fellowship within the program "Science without Borders".

REFERENCES

- Ahn, C. P., Alexandroff, R., Allende Prieto, C., et al. 2014, *ApJS*, 211, 17
- Allende Prieto, C., Majewski, S. R., Schiavon, R., et al. 2008 *Astronomical Society*, 329, 1018
- Amaral, L. H., & Lépine, J. R. D. 1997, *MNRAS*, 286, 885
- Amôres, E. B., Lépine, J. R. D., & Mishurov, Y. N. 2009, *MNRAS*, 400, 1768
- Anders, F., Chiappini, C., Santiago, B. X., et al. 2014, *A&A*, 564, A115
- Antoja, T., Valenzuela, O., Pichardo, B., et al. 2009, *ApJ*, 700, L78
- Aumer, M., & Binney, J. J. 2009, *IAU Symposium*, 254, 6P
- Barros, D. A., Lépine, J. R. D., & Junqueira, T. C. 2013, *MNRAS*, 435, 2299
- Binney, J., & Tremaine, S. 2008, *Galactic Dynamics: Second Edition*, by James Binney and Scott Tremaine. ISBN 978-0-691-13026-2 (HB). Published by Princeton University Press, Princeton, NJ USA, 2008.
- Bobylev, V. V., & Bajkova, A. T. 2010, *MNRAS*, 408, 1788
- Burton, W. B. 1971, *A&A*, 10, 76
- Contopoulos, G., & Grosbøl, P. 1986, *A&A*, 155, 11
- Creze, M., & Mennessier, M. O. 1973, *A&A*, 27, 281
- Dalton G., et al., 2012, *SPIE*, 8446
- de Jong, R. S., Bellido-Tirado, O., Chiappini, C., et al. 2012, *SPIE*, 8446,
- de Bruijne J. H. J., 2012, *Ap&SS*, 341, 31
- Dias, W. S., Alessi, B. S., Moitinho, A., & Lépine, J. R. D. 2002, *A&A*, 389, 871
- Dias, W. S., & Lépine, J. R. D. 2005, *ApJ*, 629, 825
- Drimmel, R. 2000, *A&A*, 358, L13
- Eisenstein, D. J., Weinberg, D. H., Agol, E., et al. 2011, *AJ*, 142, 72
- Fernández, D., Figueras, F., & Torra, J. 2001, *A&A*, 372, 833
- Fich, M., Blitz, L., & Stark, A. A. 1989, *Apj*, 342, 272
- Gerhard, O. 2011, *Memorie della Societa Astronomica Italiana Supplementi*, 18, 185
- Gilmore G., et al., 2012, *Msngr*, 147, 25
- Grand, R. J. J., Kawata, D., & Cropper, M. 2014, *MNRAS*, 439, 623
- Johnson, D. R. H., & Soderblom, D. R. 1987, *AJ*, 93, 864
- Junqueira, T. C., Lépine, J. R. D., Braga, C. A. S., & Barros, D. A. 2013, *A&A*, 550, A91
- Kalnajs, A. J. 1973, *Proceedings of the Astronomical Society of Australia*, 2, 174
- Lépine, J. R. D., & Leroy, P. 2000, *MNRAS*, 313, 263
- Lépine, J. R. D., Dias, W. S., & Mishurov, Y. 2008, *MNRAS*, 386, 2081
- Lépine, J. R. D., Roman-Lopes, A., Abraham, Z., Junqueira, T. C., & Mishurov, Y. N. 2011a, *MNRAS*, 414, 1607
- Lépine, J. R. D., Cruz, P., Scarano, S., Jr., et al. 2011b, *MNRAS*, 417, 698
- Lin, C. C., & Shu, F. H. 1964, *ApJ*, 140, 646
- Lynga, G., & Palous, J. 1987, *A&A*, 188, 35
- Lynden-Bell, D., & Kalnajs, A. J. 1972, *MNRAS*, 157, 1
- Majewski, S. R., & The SDSS-III/APOGEE Collaboration 2014, *American Astronomical Society Meeting Abstracts #223*, 223, #440.01
- Marochnik, L. S., Mishurov, Y. N., & Suchkov, A. A. 1972, *Ap&SS*, 19, 285
- Martos, M., Hernandez, X., Yáñez, M., Moreno, E., & Pichardo, B. 2004, *MNRAS*, 350, L47
- Masset, F., & Tagger, M. 1997, *A&A*, 322, 442
- Mermilliod, J.-C., Andersen, J., Nordstroem, B., & Mayor, M. 1995, *A&A*, 299, 53
- Merrifield, M. R., Rand, R. J., & Meidt, S. E. 2006, *MNRAS*, 366, L17
- Minchev, I., & Quillen, A. C. 2006, *MNRAS*, 368, 623
- Minchev, I., Famaey, B., Quillen, A. C., et al. 2012, *A&A*, 548, A126
- Minchev, I., Chiappini, C., & Martig, M. 2013, *A&A*, 558, AA9
- Minchev, I., Chiappini, C., & Martig, M. 2014, *A&A*, 572, AA92
- Mishurov, Y. N., Pavlovskaya, E. D., & Suchkov, A. A. 1979, *Soviet Ast.*, 23, 147
- Mishurov, Y. N., Zenina, I. A., Dambis, A. K., Mel'Nik, A. M., & Rastorguev, A. S. 1997, *A&A*, 323, 775
- Mishurov, Y. N., & Zenina, I. A. 1999, *A&A*, 341, 81
- Naoz, S., & Shaviv, N. J. 2007, *New Astron.*, 12, 410
- Patsis, P. A. 2006, *MNRAS*, 369, L56
- Paunzen, E., & Netopil, M. 2006, *MNRAS*, 371, 1641
- Pichardo, B., Martos, M., Moreno, E., & Espresate, J. 2003, *ApJ*, 582, 230
- Piffl, T., Binney, J., McMillan, P. J., et al. 2014, *MNRAS*, 445, 3133
- Quillen, A. C., & Minchev, I. 2005, *AJ*, 130, 576
- Quillen, A. C., Dougherty, J., Bagley, M. B., Minchev, I., & Comparella, J. 2011, *MNRAS*, 417, 762
- Santiago, B. X., Brauer, D. E., Anders, F., et al. 2015, *arXiv:1501.05500*
- Scarano, S., & Lépine, J. R. D. 2013, *MNRAS*, 428, 625
- Schönrich, R., Binney, J., & Dehnen, W. 2010, *MNRAS*, 403, 1829
- Sellwood, J. A., & Binney, J. J. 2002, *MNRAS*, 336, 785
- Sellwood, J. A. 2014, *Reviews of Modern Physics*, 86, 1
- Siebert, A., Famaey, B., Binney, J., et al. 2012, *MNRAS*, 425, 2335
- Silva, M. D. V., & Napiwotzki, R. 2013, *MNRAS*, 431, 502
- Sobeck, J., Majewski, S., Hearty, F., et al. 2014, *American Astronomical Society Meeting Abstracts #223*, 223, #440.06
- Steinmetz, M., Zwitter, T., Siebert, A., et al. 2006, *AJ*, 132, 1645
- Toomre, A. 1981, *Structure and Evolution of Normal Galaxies*, 111
- Vallée, J. P. 2014, *AJ*, 148, 5
- Yanny B., et al., 2009, *AJ*, 137, 4377

This paper has been typeset from a \TeX / \LaTeX file prepared by the author.